Microelectronic Engineering 89 (2012) 133–137

Contents lists available at ScienceDirect

Microelectronic Engineering

journal homepage: www.elsevier.com/locate/mee

# Linear inductive antenna design for large area flat panel display plasma processing

K.N. Kim [a], J.H. Lim [a], H.B. Jeong [a], G.Y. Yeom [a,b,*], S.H. Lee [c], J.K. Lee [c]

[a] Department of Materials Science and Engineering, Sungkyunkwan University, Suwon, Gyeunggi-do 440-746, South Korea
[b] SKKU Advanced Institute of Nanotechnology (SAINT), Sungkyunkwan University, Suwon, Gyeunggi-do 440-746, South Korea
[c] Department of Electronic and Electrical Engineering, Pohang University of Science and Technology, Pohang 790-784, South Korea

A R T I C L E I N F O

*Article history:*
Available online 23 July 2011

*Keywords:*
Plasma
Etching
Uniformity

A B S T R A C T

Two different internal-type linear inductive antenna arrangements, that is, parallel and anti-parallel antenna arrangements having different current directions between adjacent antennas were investigated for a large area plasma source having the size of 1020 mm × 830 mm. The electric field profile and plasma density of Ar calculated by the F2L code showed consistent results with the experimental results on the plasma density and processing results. The results showed that the anti-parallel antenna arrangement showed better plasma uniformity compared to the parallel antenna arrangement due to the destructive $E_z$-field between adjacent antennas even though the destructive $E_z$-field decreases the plasma density at the center of the chamber.

© 2011 Elsevier B.V. All rights reserved.

## 1. Introduction

For years, in order to improve production efficiency, large-diameter silicon wafer substrates and large-area glass substrates have been adopted in semiconductor device and flat panel display (FPD) industries. Especially, high-density and large area plasma processing technologies are indispensable for FPD processing [1–4]. Main trend of the substrate size in flat panel display is expected to expand to 3000 × 3320 mm$^2$ (11th generation) in the near future [4].

The inductively coupled plasma (ICP) source with externally spiral-type antennas [5,6], which is widely studied for the plasma sources in semiconductor processing (~300 mm in diameter), has several limitations for the application of FPD manufacturing processes having the extremely large substrate size (>1000 mm in one side). Due to the increase of the thickness of the dielectric material separating the ICP antenna and the plasma, and due to the large inductance of the spiral antennas with the scale-up to larger areas, the rf voltage induced on the antenna is increased significantly, and which can lead to be more capacitively coupled with a low efficient plasma production [7–9]. Therefore, new concepts of inductive antenna designs with high efficiency are required to overcome the limitations in the plasma processing for the extremely large area. One of the solutions resolving the above problems is to use internal-type ICPs, which could effectively exclude some of the problems of the external-type ICPs related to the cost and the thickness of dielectric materials separating the ICP antenna and the plasma when scaling to large areas [10–12]. However, when the internal-type method is used, and problems like uniformity, impedance control, standing wave effect, etc. Still remain to be resolved when the source is extended to a large size as studied by many researchers [13,14].

In this study, as the internal ICP antennas, two different ICP antenna arrangements, parallel antenna arrangement (comb type) and anti-parallel antenna arrangement (double-comb type) which have different power connection arrangement between adjacent linear antennas were investigated as the large area ICP sources. These two types of antennas were chosen to reduce the standing wave effect due to their short antenna length. To study the effect of the antenna arrangement on better and more effective plasma generation, a simulation technique has been carried out in addition to the experimental study.

## 2. Experiments

A schematic diagram of the internal-type linear-antenna ICP source used in this study is shown in Fig. 1. The process chamber is designed as a rectangular shape for the FPD applications and is made of stainless steel. The inner size of the chamber is 1020 mm × 830 mm × 440 mm. As shown in this figure, five parallel-connected antennas (comb type antenna; upper antenna figure) or anti-parallel-connected antennas (double-comb type antenna; lower antenna figure) were embedded in the vacuum chamber as the antenna configuration. One end of the each antenna was connected to the rf power supply while the other end of the each antenna as connected to ground. The length of the each linear antenna is 1240 mm and the distance between the neighboring antennas is 160 mm. The antenna is made of 10 mm diameter

* Corresponding author at: Department of Materials Science and Engineering, Sungkyunkwan University, Suwon, Gyeunggi-do 440-746, South Korea.
*E-mail address:* gyyeom@skku.edu (G.Y. Yeom).

0167-9317/$ - see front matter © 2011 Elsevier B.V. All rights reserved.
doi:10.1016/j.mee.2011.07.003

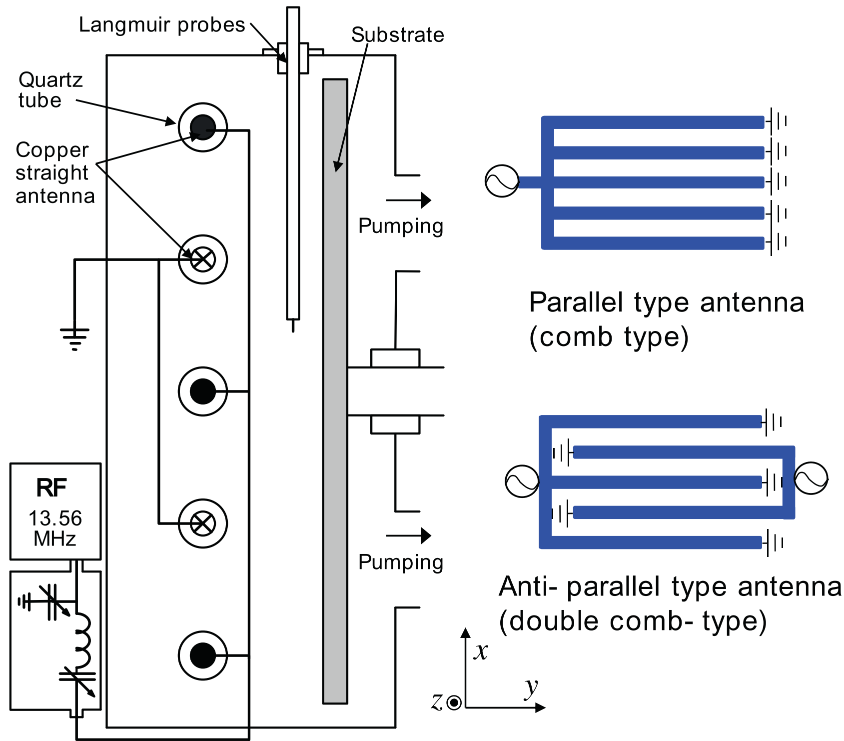


**Fig. 1.** Schematic diagram of inductively coupled plasma system used in the experiment, and the two different configurations of the internal linear inductive antenna arrangement (parallel and anti-parallel antenna arrangements).

copper tubing and the outside of the copper tubing is coaxially covered with quartz tubing. The outer diameter of the quartz tubing is 15 mm and the thickness of the quartz is 2 mm. 13.56 MHz (0–5000 W) rf power was fed to the antenna through a conventional L-type matching network.

Ion saturation current was measured along the vertical centerline of the chamber as a measure of plasma uniformity using a home-made Langmuir probe. Plasma characteristics were also measured using a commercial Langmuir probe (Hiden Analytical Inc., ESP) located 7.5 cm below the antenna. The etch characteristics of $SiO_2$ and photoresist (AZ-GXR601) films deposited on a sodalime glass were investigated for 5000 W of rf power using the water-cooled substrate holder installed 5 cm below the source and connected to a separate rf power supply (12.56 MHz, 0–2000 W) through a separate matching network to supply bias voltages to the substrate. $SiO_2$ was etched using 15 mTorr of $SF_6$ and by applying −35 V of bias voltage to the substrate holder while photoresist was etched using 15 mTorr of $O_2$ and by applying −60 V of bias voltage. A simulation of the plasma was carried out using a two dimensional fluid code (F2L code) and was compared with the experimental results to figure out the results obtained in the experiment.

## 3. Results and discussion

In an ICP source, the spatial distribution of the rf induced electric field determines the power absorbed by the plasma, and ion density profiles follow the absorbed power shape [14]. Therefore, there is close correlation between the spatial distribution of the induction component of the electric field and the plasma uniformity which is one of the key factors in the FPD processing. To investigate the effect of the power connection arrangement to the adjacent antenna on the plasma uniformity, the spatial distributions of the induced electric field ($E_z$: the induced electric field in the direction parallel to the antenna line) and plasma density for the two different power connection arrangements, that is, the parallel antenna arrangement (comb type) and the anti-parallel antenna arrangement (double-comb type), were calculated for Ar by the F2L code, and the results are shown in Fig. 2. The total area of the simulation domain was 20 cm × 10 cm and the distance between the adjacent antennas was 4 cm in order to distinguish the effect of current flowing direction for the parallel and anti-parallel antenna arrangements. Fig. 2a and b show the schematic diagrams of the resulting induced electric field ($E_z$) for the parallel antenna arrangement and the anti-parallel antenna arrangement, respectively. In the case of the parallel antenna arrangement, the current to flowing one antenna is the same direction with the current flowing on the adjacent antenna. In the case of the anti-parallel antenna arrangement, however, the direction of the current flowing on one antenna is the opposite direction with that on the adjacent antenna.

The $E_z$ field at the each antenna position was calculated by the F2L code. To obtain the $E_z$ field, wave equations for the transmission line were solved using the following voltage and current to the antenna;

$$V(z) = \frac{I_L}{2}[(Z_L + Z_o)e^{\gamma(l-z)} + (Z_L - Z_o)e^{\gamma(l-z)}] \quad (1)$$

$$I(z) = \frac{I_L}{2Z_o}[(Z_L + Z_o)e^{\gamma(l-z)} - (Z_L - Z_o)e^{\gamma(l-z)}] \quad (2)$$

where, $V(z)$ and $I(z)$ are the voltage and current along the antenna line, $Z_0$ is the characteristic impedance, $Z_L$ is the load impedance $\left(= \left(\frac{V}{I}\right)_{z=l} = \left(\frac{V_L}{I_L}\right) = Z_L,\ l \text{ is the total antenna length}\right)$, $\gamma$ is the propagation constant (=$\alpha + j\beta$), and $I_L$ is the load current. The calculated results are shown in Fig. 2c and d for $E_z$-field and Fig. 2e and f for plasma density, for the parallel antenna arrangement and the anti-parallel antenna arrangement, respectively. For the calculation of plasma density, 15 mTorr of Ar, inductive power of 1 kW were used as the simulation conditions. As shown in the Fig. 2c, in the case of the parallel antenna arrangement, the normalized $E_z$-field

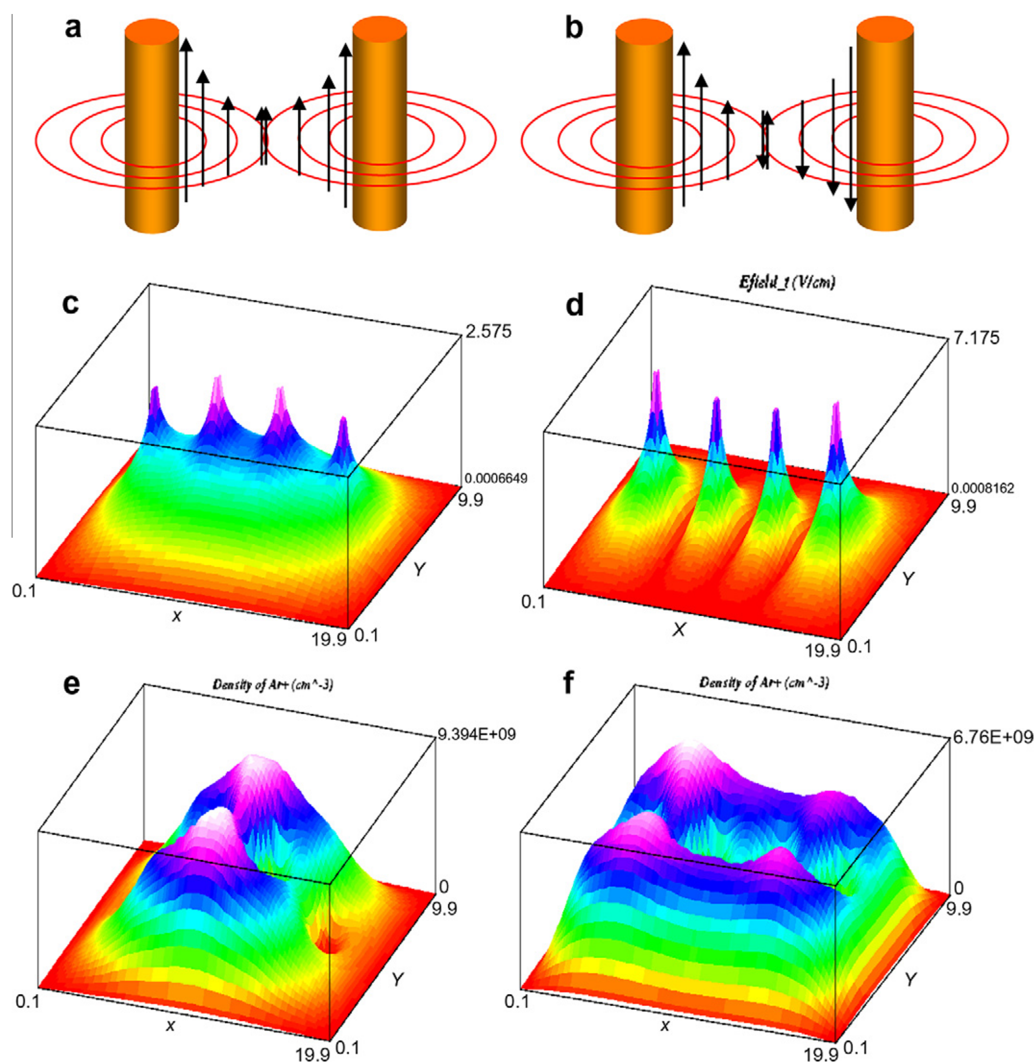


**Fig. 2.** Schematic diagrams of antenna, normalized $E_z$-field profile, and $Ar^+$ density ($cm^{-3}$) profile ((a, c, e): parallel antenna arrangement, (b, d, f): anti-parallel antenna arrangement).

appears as a convex shape because the electric field generated by each antenna was constructively overlapped in the middle as shown in Fig. 2a. In the case of anti-parallel antenna arrangement, however, the $E_z$-field appears as a concave shape because the electric field generated by each antenna was destructively offset in the middle as shown in Fig. 2b. However, as shown in the Fig. 2e and f, the spatial distribution of plasma density is less fluctuating for the anti-parallel antenna arrangement case compared to that of the parallel antenna case, which indicates more uniform plasma for the anti-parallel antenna arrangement case. That is, although there is a destructive $E_z$-field effect in the anti-parallel antenna arrangement, this arrangement method is more desirable for larger substrate processing because of the characteristic of the $E_z$-field.

To prove the simulation results experimentally, the internal antennas were located in parallel directions using a 4th generation reaction chamber (1020 mm × 830 mm) and the rf power was connected two different methods as shown in Fig. 1, that is, the power was connected to the same side of the antenna ends to form the parallel antenna arrangement (comb type) or the power was connected to the alternate side of the antenna ends to form the anti-parallel antenna arrangement (double-comb type). The antenna arrangements used in this study were also useful in reducing the standing wave effect due to the short length of the antenna line from the rf power input to the ground. Fig. 3 shows the ion saturation current profiles experimentally measured 7.5 cm below the internal antennas (a) for the parallel antenna arrangement and (b) for the anti-parallel antenna arrangement using the homemade Langmuir probe for the rf power of 5 kW and at 15 mTorr Ar. The ion saturation current profile was used as a measure of relative plasma uniformity. The Langmuir probe was scanned along the centerline of the substrate width (the substrate size is 880 mm length × 660 mm width). The probe was scanned across the antenna lines (that is, along the 660 mm width) which are considered to show worse plasma uniformity compared to that measured along the antenna line (that is, along the 880 mm length). As shown in Fig. 3a, in the case of the parallel antenna arrangement, ion saturation current profile showed a convex shape because of the constructive overlapping of the electric filed in the middle as shown in Fig. 2a. This constructively overlapping of the electric field in the middle area resulted in the rapid decrease of ion current at the chamber edge area, therefore, the plasma uniformity of 22% was obtained. In the case of anti-parallel antenna arrangement, however, ion saturation current profile was more uniform than that of the parallel antenna arrangement similar to the simulation result shown in Fig. 2f, and the plasma uniformity of about 8% could be obtained. This result appears to be related to the destructively offset of the electric field generated by each antenna as shown in Fig. 2b. In this case, a hump-shaped high den-

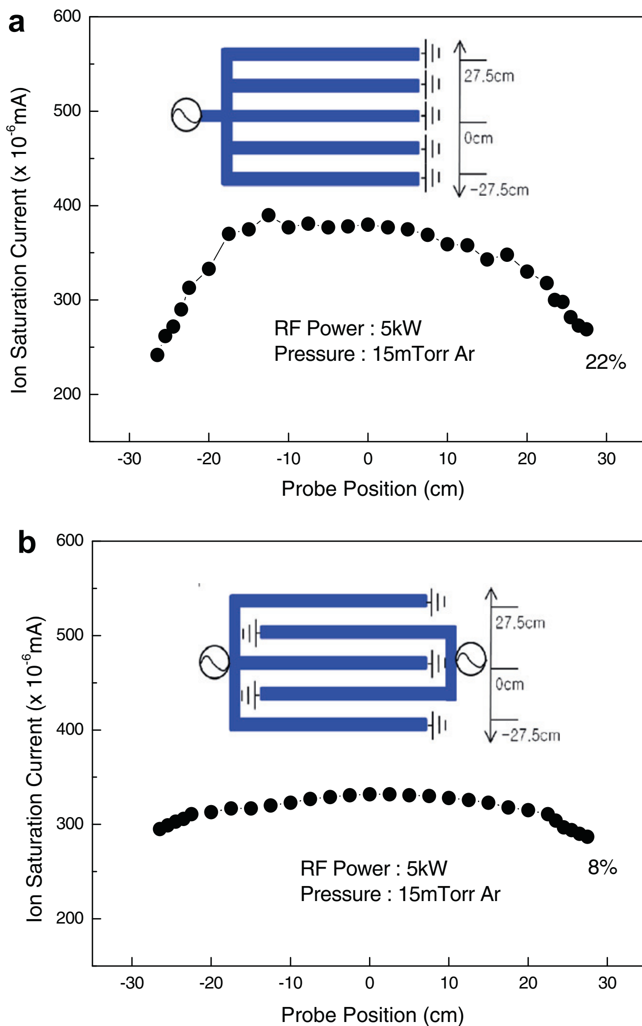


**Fig. 3.** Ion saturation current profile measured using a Langmuir probe 7.5 m below the each antenna for 5 kW of rf power and at 15 mTorr Ar.

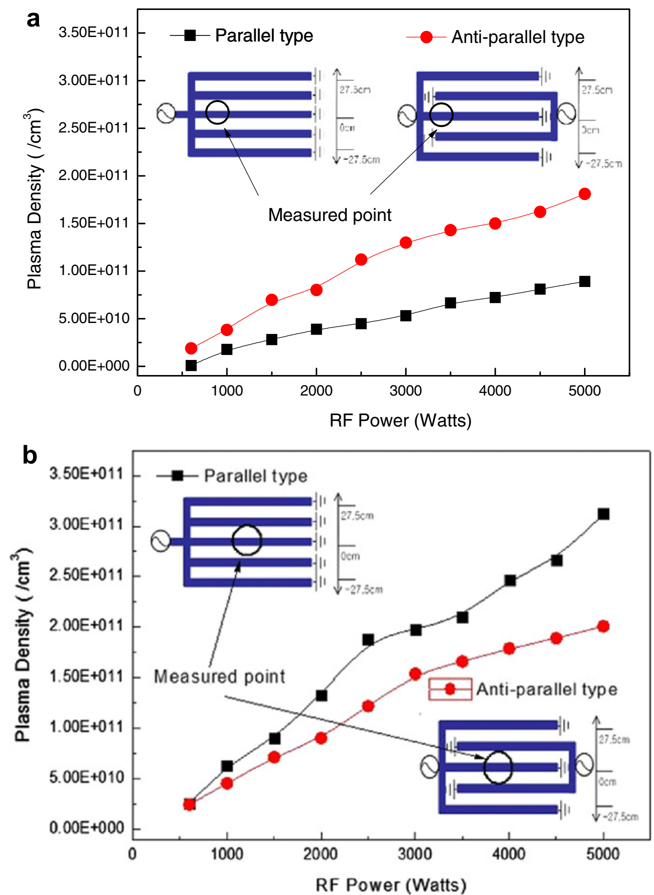


**Fig. 4.** Ar ion density measured by a Langmuir probe at 7.5 m below the antenna (a) at the edge and (b) at the center of the processing chamber for both the parallel antenna arrangement and the anti-parallel antenna arrangement as a function of rf power from 600 to 5000 W for 15 mTorr Ar.

sity plasma region in the middle of the chamber is not observed, but, the plasma uniformity was improved by not showing significant decreased plasma density in the chamber edge region. Actually, to compare the plasma uniformity and etch uniformity, the etch uniformity on the substrate size of 660 mm $\times$ 880 mm is studied, and 7% non-uniformity is obtained (not shown).

Fig. 4 show the effect of rf power on the Ar plasma densities for the parallel antenna arrangement and the anti-parallel antenna arrangement measured by the commercial Langmuir probe. The rf power was varied from 600 to 5000 W. Ar plasma densities were measured (a) at the edge of the chamber and (b) at the center of the chamber. As shown in the figure, the increase of rf power to the antennas increased the plasma densities almost linearly without saturation for all of the cases. For the parallel antenna arrangement, the plasma density at the edge of the chamber increased higher than $1 \times 10^{11}/cm^3$ when the rf power is close to 5000 W while that at the center of the chamber increased higher than $1 \times 10^{11}/cm^3$ when the rf power is close to 1500 W, and, at 5000 W, the plasma density at the center of the chamber was close to $3.1 \times 10^{11}/cm^3$. In the case of the anti-parallel antenna arrangement, the plasma density increased higher than $1 \times 10^{11}/cm^3$ when the rf power was higher than 2000 W for both at the center and edge of the chamber and, when the rf power was increased to 5000 W, the edge of the chamber showed the plasma density of about $1.8 \times 10^{11}/cm^3$ while the center showed about $2.0 \times 10^{11}/cm^3$. Therefore, by applying rf power higher than 2000 W, a high density plasma could be obtained even with the anti-parallel antenna arrangement and, similar to the ion saturation current measurement shown in Fig. 3, more uniform plasma densities could be obtained with the anti-parallel antenna arrangement.

In addition to the measurement of plasma density to compare with the simulation results, the etching of FPD materials such as photoresist and $SiO_2$ has been carried out to investigate the relationship between the simulation results and the actual material processing results. Etching of photoresist and $SiO_2$ was performed on the substrate area of 880 mm $\times$ 660 mm with 5000 W of rf power and by applying bias voltage to the substrate holder with a separate 12.56 MHz rf power. Photoresist was etched using 15 mTorr of $SF_6$ and by applying $-35$ V of bias voltage to the substrate holder and $SiO_2$ was etched using 15 mTorr of $O_2$ and by applying $-60$ V of bias voltage. Etch depth after 5 min of etching was measured along the 660 mm side which is the direction across the antenna lines and the results are shown in Fig. 5a and b for $SiO_2$ etching and photoresist etching, respectively. As shown in the figure, the measured $SiO_2$ etch uniformity was about 6.4% with the average etch rate of 2200 Å/min and the photoresist etch uniformity was about 7.5% with the average etch rate of 3500 Å/min similar to the ion saturation current profiles measured with the Langmuir probe shown in Fig. 4. Therefore, the processing results similar to the simulation results could be obtained, and, for the internal-type linear antenna arrangement, the anti-parallel antenna arrangement showed much better processing uniformity compared to the parallel antenna arrangement.

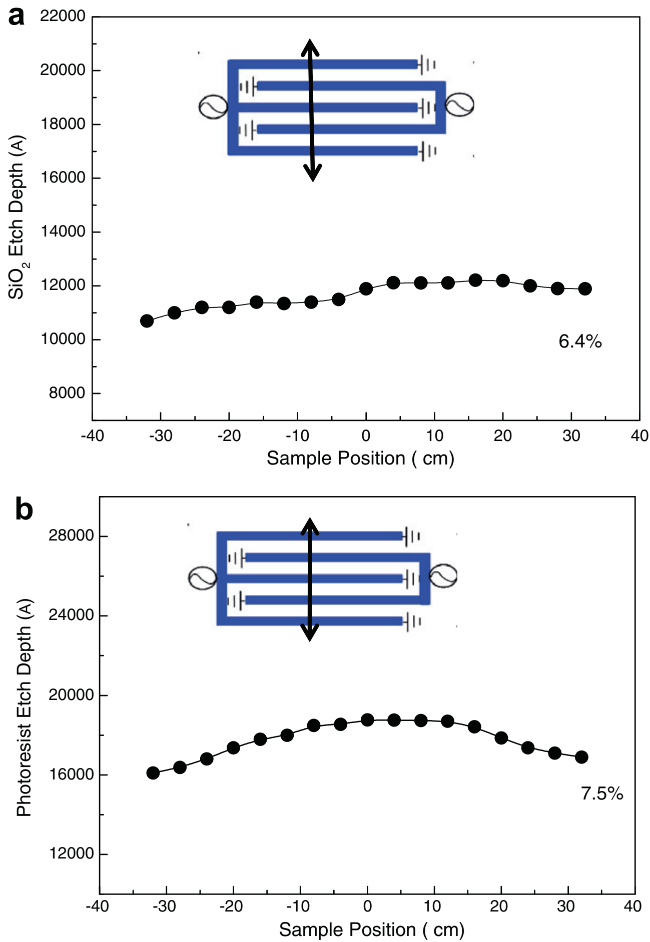


**Fig. 5.** (a) Etch depth of $SiO_2$ measured at 5000 W of rf power, −35 V of dc-bias voltage, and 15 mTorr of $SF_6$. (b) Etch depth of photoresist measured at 5000 W of rf power, −60 V of dc-bias voltage, and 15 mTorr of $O_2$.

## 4. Conclusions

The effect of internal-type linear antenna arrangements, that is, a parallel antenna arrangement and an anti-parallel antenna arrangement, on the characteristics of the plasmas and the processing uniformity was investigated for a large-area plasma source applied to FPD processing. The $E_z$-field and plasma density were calculated by using the F2L code for the parallel and anti-parallel antenna arrangements, and the anti-parallel antenna arrangement showed the characteristics more desirable for larger plasma processing because of the characteristic of the spatial distribution of $E_z$-field and plasma caused by the destructive $E$-field effect in the anti-parallel antenna arrangement. Similar results could be obtained when the plasma uniformity was experimentally measured on the 4th generation plasma source (1020 mm × 830 mm). By using the anti-parallel antenna arrangement, the plasma density higher than $2 \times 10^{11}$ cm$^{-3}$ with the plasma uniformity less than 8% could be obtained for 15 mTorr Ar and at 5000 W of rf power. Also, when the photoresist and $SiO_2$ were etched, similar etch uniformities less than 7.5% could be obtained.

## Acknowledgment

This work was partly supported by the IT R&D program of MKE/KEIT (S-2010-1436-000), Development of Oxide Trench Etcher beyond 25 nm, the Korea Industrial Technology Foundation (KOTEF) through the Human Resource Training Project for Strategic Technology and Basic Science Research Program through the National Research Foundation of Korea (NRF) funded by the Ministry of Education, Science and Technology (2010-0015035).

## References

[1] J. Holland, M. Barnes, A. Demos, T. Ni, P. Shufflebotham, W. Yao, SID Sym. Digest 27 (1996) 526.
[2] F. Heinrich, U. Banzlger, A. Jentzsch, G. Neumann, C. Huth, J. Vac. Sci. Technol. B 14 (1996) 2000.
[3] H. Takei, H. Kawamura, Y. Ohta, R. Gardner, SID 98 Digest, 1102 (1998).
[4] J. Schmitt, M. Elyaakoubi, L. Sansonnens, Plasma Sources Sci. Technol. 11 (2002) A206.
[5] W.Z. Collison, T.Q. Ni, M.S. Barnes, J. Vac. Sci. Technol. A 16 (1998) 100.
[6] S.S. Kim, H.Y. Chang, C.S. Chang, N.S. Yoon, Appl. Phys. Lett. 77 (2000) 492.
[7] Z. Yu, D. Shaw, P. Gonzales, G.J. Collins, J. Vac. Sci. Technol. A 13 (1995) 503.
[8] J.H. Kim, H.J. Lee, Y.T. Kim, J.H. Joo, K.W. Whang, J. Vac. Sci. Technol. A 15 (1997) 564.
[9] T. Meziani, P. Colpo, F. Rossi, Plasma Sources Sci. Technol. 10 (2001) 276.
[10] K. Suzuki, K. Nakamura, H. Ohkubo, H. Sugai, Plasma Sources Sci. Technol. 7 (1998) 13.
[11] Y. Wu, M.A. Lieberman, Appl. Phys. Lett. 72 (1998) 777.
[12] M. Kanoh, K. Suzuki, J. Tonotani, K. Aoki, M. Yamage, Jpn. J. Appl. Phys. Part 1 40 (2001) 5419.
[13] H. Deguchi, H. Yoneda, K. Kato, K. Kubota, T. Hayashi, K. Ogata, A. Ebe, K. Takenaka, Y. Setsuhara, Jpn. J. Appl. Phys. 45 (2006) 10B.
[14] K.N. Kim, G.Y. Yeom, J. Korean Phys. Soc. 48 (2006) 256.